Int. J. Solids Structures Vol. 30, No. 10, pp. 1313–1329, 1993
Printed in Great Britain

0020–7683/93 $6.00+ .00

ANALYSES OF THE FIBER PUSH-OUT TEST

A. DOLLAR and P. S. STEIF
Department of Mechanical Engineering, Carnegie Mellon University, Pittsburgh, PA 15213, U.S.A.

and

Y. C. WANG and C. Y. HUI
Department of Theoretical and Applied Mechanics, Cornell University, Ithaca, NY 14853, U.S.A.

(*Received* 4 *May* 1992; *in revised form* 9 *November* 1992)

Abstract—A two-dimensional model of the fiber push-out test is considered. Two distinct methods of analysis are independently employed in solving the problem, and their accuracy is indicated by the virtual coincidence of the results. Interfacial debonding is assumed to be characterized by a cohesive zone model, and subsequent slippage obeys a Coulomb friction law. We have found that the results depart from those of the more commonly employed fracture-mechanics approach, if the cohesive zone size is of the order of the fiber diameter. The accuracy of various approximate analyses is discussed.

1. INTRODUCTION

The nature of the fiber–matrix interface is widely agreed to have a major influence on the strength and toughness of ceramic–matrix composites. As a means of independently measuring the response of the interface to stress, various interface tests have been suggested. The tests most often used to measure interface strength in ceramic–matrix composites are the micro-indentation push-in test (Marshall, 1984; Grande *et al.*, 1988) and the push-out test (Laughner *et al.*, 1986; Brun and Singh, 1988; Bright *et al.*, 1989); the pull-out test has also been used (Deshmukh and Coyle, 1988; Griffin *et al.*, 1988) though to a lesser extent. In these tests the force applied to the fiber is measured as a function of time; occasionally, the motion of the fiber is also tracked as a function of time. The results of these tests are then interpreted by appealing to a mechanics analysis which relates the measured force to a local or average shear stress.

Herein, we focus on the fiber push-out test. In this test (see Fig. 1), a thin slice of the composite, cut normal to the fiber direction, is placed on a platform, and a micro-indentor is brought in contact with a fiber on the upper surface. The indentor is then forced to push on the fiber, generally under displacement control. The platform contains either a hole or a slot, which permits the fiber to be pushed out. As the indentor descends, the load increases and reaches some maximum value. After decreasing, the load eventually achieves roughly a steady value. A schematic of such a typical load–displacement curve is also shown in Fig. 1. The broad interpretation of such a load–displacement curve is that a higher level of interfacial resistance needs to be overcome to produce debonding, after which there is only resistance of a frictional nature to fiber sliding. More specifically, the initial deviation from linearity has been associated with initiation of interfacial debonding at the top of the

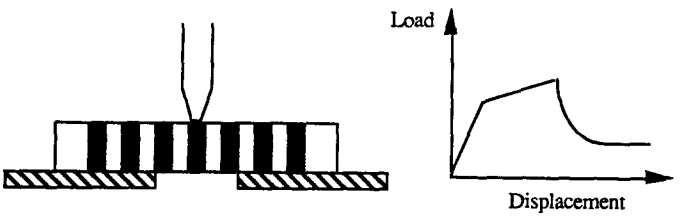

Fig. 1. Schematic of push-out test configuration and typical load–displacement curve.

specimen, and the peak has been associated with complete debonding, that is the fiber protruding out of the bottom of the specimen (Eldridge *et al.*, 1991).

In general, the mechanical analyses employed in interpreting the results of interface tests are modifications of shear lag methods and tend to be rather approximate. Just two examples of such analyses are Marshall and Oliver's (1987) analysis of the push-in test and the analysis by Bright *et al.* (1989) of the push-out test. Most experimentalists take an even simpler approach to interpreting the test. For example, a debond stress, τ_d, is computed according to

$$\tau_d = \frac{F_{peak}}{2\pi Rh}, \tag{1}$$

where F_{peak} is the peak load, h is the specimen thickness and R is the fiber diameter. A friction stress, τ_f, is computed according to

$$\tau_f = \frac{F_{ss}}{2\pi Rh}, \tag{2}$$

where F_{ss} is the steady load necessary to produce sliding.

The analyses presented here form part of an investigation into the relationship between a composite's interfacial properties and the load–displacement trace from a push-out test. This investigation is intended ultimately to yield sufficiently accurate stress analyses of model configurations representing the push-out test that the interface parameters can be reliably extracted from the load–displacement trace. Unfortunately, even model problems tend to be extremely complex with boundaries at finite distances, as well as displacement discontinuities along interfaces. It is likely that finite element computations will eventually be necessary to carry out the full three-dimensional analysis. In the meantime, however, consideration of the analogous two-dimensional problem can serve several purposes. It can give us preliminary insight into the dependence on various material and geometric parameters. In addition, it can form the basis on which to test a finite element method's accuracy.

This paper is devoted, therefore, to the development of highly accurate solutions to a two-dimensional problem analogous to the fiber push-out test. Since even the two-dimensional problem is extemely complex, we have chosen to attack it independently (at Carnegie Mellon University and at Cornell University) using two rather distinct methods of analysis. These methods are presented in some detail. The results of these methods will give insight into the influence of a number of relevant variables and will permit the validity of various approximate approaches to be assessed.

2. PROBLEM STATEMENT

The model two-dimensional problem features the infinite strip $-\infty < x < \infty$, $0 < y < h$, which is composed of the matrix occupying the region $-\infty < x < -a$ and $a < x < \infty$, and the fiber occupying the region $-a < x < a$ [see Fig. 2(a)]. The effect of a

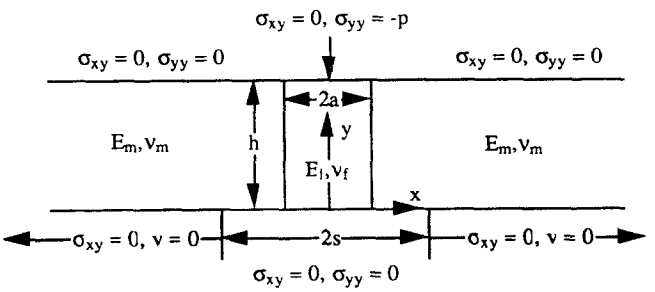

Fig. 2(a). Model two-dimensional problem representing push-out test.

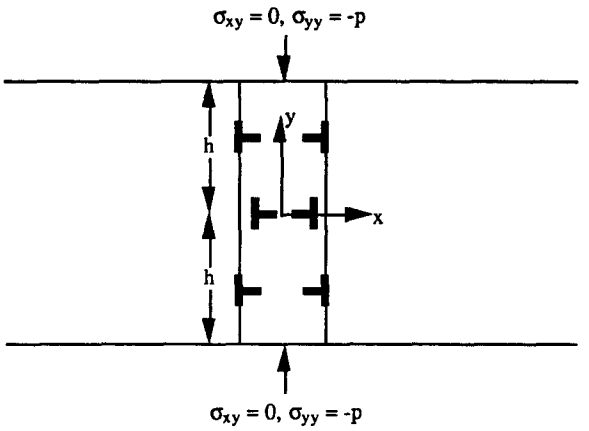

Fig. 2(b). Symmetries in dislocation distribution (Method I).

hard, flat indentor, which is typically 10–30% narrower than the fiber, is simulated by applying a uniform pressure p over the fiber at $y = h$. (Previous work has suggested that this is generally a reasonable approximation, and becomes increasingly accurate as the debonded zone extends to several fiber diameters.) Otherwise, zero tractions are applied to the upper surface $y = h$. The strip is resting on a rigid, smooth substrate containing a gap along $-s < x < s$, $y = 0$ through which the fiber can be pushed out (for clearance, s must be greater than a). The materials are assumed to be linear elastic and isotropic.

Within the present framework, the interface between the fiber and matrix can be modeled, in principle, using any relation between relative displacements and tractions. As mentioned above, this test is typically applied to ceramic–matrix composites which have relatively weak interfaces. To model an interface which is apparently typical of these materials, we will assume that the interface is capable of debonding under appropriate conditions detailed below, after which slipping occurs according to a Coulomb friction law.

More specifically, once debonding has occurred at some point, that point of the interface is either opening, sticking or slipping; these conditions are expressed mathematically (for the interface $x = a$) by:

$$\text{stick condition} \quad \sigma < 0, \quad |\tau| < \mu|\sigma|, \quad \frac{\mathrm{d}\Delta v}{\mathrm{d}t} = 0, \quad \Delta u = \frac{\mathrm{d}\Delta u}{\mathrm{d}t} = 0, \tag{3a}$$

$$\text{slip condition} \quad \sigma < 0, \quad |\tau| = \mu|\sigma|, \quad \operatorname{sgn}\left(\frac{\mathrm{d}\Delta v}{\mathrm{d}t}\right) = \operatorname{sgn}(\tau), \quad \Delta u = \frac{\mathrm{d}\Delta u}{\mathrm{d}t} = 0, \tag{3b}$$

$$\text{open condition} \quad \sigma = \tau = 0, \quad \Delta u > 0, \tag{3c}$$

with

$$\sigma = \sigma_{xx}, \quad \tau = \sigma_{xy},$$

$$\Delta u = \lim_{\varepsilon \to 0^+} [u(a+\varepsilon, y) - u(a-\varepsilon, y)],$$

$$\Delta v = \lim_{\varepsilon \to 0^+} [v(a+\varepsilon, y) - v(a-\varepsilon, y)].$$

In these equations, u and v denote the x- and y-components of displacement, respectively, σ with appropriate subscripts denotes the components of stress, μ is the friction coefficient, and $\mathrm{d}(\ )/\mathrm{d}t$ denotes the derivative with respect to a time-like parameter that increases as the loading proceeds. The condition $\operatorname{sgn}(\mathrm{d}g/\mathrm{d}t) = \operatorname{sgn}(\tau)$ corresponds to positive energy dissipation, which requires the slippage to be in the same direction as the shear stress. In applying eqns (3), one must be careful to use the total stresses, including any residual stresses, which we assume to be present; in particular, a residual compressive stress σ_0 is

presumed to exist at the interface. Thus, two parameters characterize each point on the debonded portion of the interface: σ_0 and μ.

The debonding is captured by a specific form of a Barenblatt (1962) cohesive zone model, an approach which offers some advantages over more commonly used models for debonding (Steif and Dollar, 1992). Relative motion δ at the interface can begin when the shear stress reaches a critical value τ^*. The interface can suffer relative motion under the stress τ^*, until δ reaches the critical value δ^*. For δ greater than δ^*, the stress is given by the friction law (3). A key issue discussed below is the connection between results based on a cohesive zone model and results based on the more commonly used fracture-mechanics approach to debonding which simply involves a mode II debonding energy.

3. METHODS OF ANALYSIS

Two distinct methods of analysing the push-out test, both leading to sets of integral equations, are presented here. The first method can only handle the case of equal fiber and matrix elastic moduli, whereas the second method is also capable of treating cases in which the elastic moduli are different. The first method is specifically devised for the geometry of the present problem, in contrast to the second method which is a far more general technique for treating two-dimensional elasticity problems featuring internal surfaces of displacement discontinuity and finite boundaries. As will be pointed out below, these methods were found to yield very similar results, which lends much credence to their accuracy.

Method I

This method, which is restricted to equal fiber and matrix elastic moduli, exploits the shear free boundary condition on $y = 0$ to recast the problem as one of a strip of thickness $2h$, subjected to pressure p applied along $-a < x < a, y = \pm h$. The bulging out of material along $-s < x < s, y = 0$ in the original strip is precisely represented in the symmetrically loaded strip problem by a distribution of edge dislocations (Burger's vector in the y-direction) of density $b_2(x)$ along $-s < x < s, y = 0$. Note that these dislocations must be opposite in sign to those which are typically used to represent a crack which opens under a remote tension; in the symmetrically loaded strip, the dislocations correspond to *overlap* of material. Finally, following previous work by the authors (Dollar and Steif, 1988, 1989; Wang *et al.*, 1991), sling along the interfaces $x = \pm a$ is represented by dislocations of density $b_4(y)$, also with Burger's vector in the y-direction. The combination of dislocations which properly preserves all the symmetries of the problem has signs which are indicated in Fig. 2(b). (One can see the motivation for the subscripts on the dislocation densities.)

The total stress field in the strip consists of the superposition of the stresses associated with: (i) the Filon problem [see Timoshenko and Goodier (1970)] of equal and opposite uniform pressures applied to two sides of a strip; (ii) dislocations distributed along $-s < x < s, y = 0$ in a strip free of surface tractions; and, (iii) dislocations distributed along a portion of the interfaces ($x = \pm a, d < |y| < h$) in a strip free of surface tractions. This superposition can be written symbolically in the form

$$\sigma(z) = \sigma_F(z) + \int_0^s [\sigma_2(z, x') + \sigma_{2R}(z, x')]\, dx' + \int_d^h [\sigma_4(z, y') + \sigma_{4R}(z, y')]\, dy', \tag{4}$$

where $\sigma(z)$ is the total stress at some point z in the domain, $\sigma_F(z)$ is the stress associated with the Filon problem, the first integral represents the stress associated with dislocations along $-s < x < s, y = 0$, and the second integral represents the stress associated with dislocations along the interfaces at $x = a$. The contributions due to the dislocations are themselves found from a superposition procedure. Each of the integrands is split into two parts: $\sigma_2(z, x')$ and $\sigma_4(z, y')$ are solutions for the dislocation pair and the dislocation quadruple in an infinite medium, respectively; $\sigma_{2R}(z, x')$ and $\sigma_{4R}(z, y')$ are the stresses associated with relieving the tractions that these dislocations induce on the surfaces $y = \pm h$.

The stresses associated with the dislocations in the infinite medium are well known; the stresses $\sigma_F(z)$, $\sigma_{2R}(z, x')$ and $\sigma_{4R}(z, y')$ may be calculated using the Fourier transform. [In fact, the solution from which one can compute the stresses $\sigma_F(z)$ is given by Sneddon (1951).] The Fourier transform $F(\xi)$ of a function $f(x)$ is defined by (Sneddon, 1951):

$$F(\xi) = \frac{1}{\sqrt{2\pi}} \int_{-\infty}^{\infty} f(x)\, e^{i\xi x}\, dx, \tag{5}$$

and has the associated inversion formula

$$f(x) = \frac{1}{\sqrt{2\pi}} \int_{-\infty}^{\infty} F(\xi)\, e^{-i\xi x}\, d\xi. \tag{6}$$

A rather abbreviated description of the computation of $\sigma_F(z)$, $\sigma_{2R}(z, x')$ and $\sigma_{4R}(z, y')$ is given here; some of the details are left for the Appendix. In each case, the problem consists of determining the stresses in the strip when tractions σ_{xy} and σ_{yy} are prescribed along $y = \pm h$. Specifically, the tractions are either a uniform pressure over a finite segment (as in the Filon problem), or are obtained from the stresses associated with a dislocation in an infinite plane. In all cases, the tractions have the following symmetries:

$$\sigma_{yy}(x, h) = \sigma_{yy}(x, -h) = \sigma_{yy}(-x, h) = \sigma_{yy}(-x, -h), \tag{7}$$

$$\sigma_{xy}(x, h) = -\sigma_{xy}(x, -h) = -\sigma_{xy}(-x, h) = \sigma_{xy}(-x, -h). \tag{8}$$

These symmetries imply that the Fourier transform Ψ of the Airy stress function ψ must be of the general form

$$\Psi(\xi, y) = A(\xi) \cosh(|\xi| y) + B(\xi)|\xi| y \sinh(|\xi| y), \tag{9}$$

where ψ is related to the stresses according to

$$\sigma_{xx} = \frac{\partial^2 \psi}{\partial y^2}, \quad \sigma_{yy} = \frac{\partial^2 \psi}{\partial x^2}, \quad \sigma_{xy} = -\frac{\partial^2 \psi}{\partial x\, \partial y}. \tag{10}$$

Now, let $\Sigma_{xy}(\xi, h)$ and $\Sigma_{yy}(\xi, h)$ be the transforms of the boundary tractions $\sigma_{xy}(x, h)$ and $\sigma_{yy}(x, h)$. If these transforms are denoted by

$$\Sigma_{xy}(\xi, h) = F(\xi), \quad \Sigma_{yy}(\xi, h) = G(\xi) \tag{11}$$

then the coefficients $A(\xi)$ and $B(\xi)$ in eqn (9) are found to be

$$A(\xi) = \frac{\dfrac{F(\xi)}{i\xi} h \sinh(|\xi| h) + \dfrac{G(\xi)}{\xi^2} [\sinh(|\xi| h) + h|\xi| \cosh(|\xi| h)]}{h(\xi) + \cosh(|\xi| h) \sinh(|\xi| h)}, \tag{12a}$$

$$B(\xi) = \frac{\dfrac{F(\xi)}{i\xi|\xi|} \cosh(|\xi| h) + \dfrac{G(\xi)}{\xi^2} \sinh(|\xi| h)}{h(\xi) + \cosh(|\xi| h) \sinh(|\xi| h)}. \tag{12b}$$

The transform $\Psi(\xi, y)$ can then be inverted to yield the following expressions for the stress components:

$$\sigma_{xx} = \frac{1}{h}\sqrt{\frac{2}{\pi}}[2H_1(r)+2H_1(q)-qH_2(r)-rH_2(q)+I_2(r)+I_2(q)-qI_1(r)-rI_1(q)], \tag{13a}$$

$$\sigma_{yy} = \frac{1}{h}\sqrt{\frac{2}{\pi}}[qH_2(r)+rH_2(q)+I_2(r)+I_2(q)+qI_1(r)+rI_1(q)], \tag{13b}$$

$$\sigma_{xy} = \frac{1}{h}\sqrt{\frac{2}{\pi}}[H_3(r)-H_3(q)-qH_4(r)+rH_4(q)-qI_3(r)+rI_3(q)], \tag{13c}$$

where $r = 1+(y/h)$, $q = 1-(y/h)$, and the integrals I_1, I_2, I_3, H_1, H_2, H_3 and H_4, which are given in the Appendix, depend on the transformed tractions $F(\xi)$ and $G(\xi)$.

For the Filon problem, the transforms of the boundary tractions, $F_F(\xi)$ and $G_F(\xi)$, are given by

$$F_F(\xi) = 0, \tag{14a}$$

$$G_F(\xi) = -p\sqrt{\frac{2}{\pi}}\frac{\sin(\xi a)}{\xi}. \tag{14b}$$

For two dislocations, $b_2(x')$ at $(x',0)$ and $-b_2(x')$ at $(-x',0)$, the transforms of the boundary tractions, $F_2(\xi)$ and $G_2(\xi)$, are given by

$$iF_2(\xi) = \pm 2\sqrt{2\pi}\,e^{-|\xi|h}\,|\xi|h\sin(|\xi|x')b_2(x'), \tag{15a}$$

$$G_2(\xi) = -2\sqrt{2\pi}\,e^{-|\xi|h}\,(1+|\xi|h)\sin(|\xi|x')b_2(x'), \tag{15b}$$

where $i = \sqrt{-1}$, and "+" in eqn (15a) refers to $\xi > 0$ and "−" refers to $\xi > 0$.

For four dislocations, $b_4(y')$ at $(a, \pm y')$ and $-b_4(y')$ at $(-a, \pm y')$, the transforms of the boundary tractions, $F_4(\xi)$ and $G_4(\xi)$, are given by

$$iF_4(\xi) = \pm 4\sqrt{2\pi}\,e^{-|\xi|h}\sin(|\xi|a)|\xi|h[\cosh(|\xi|y') - (y'/h)\sinh(|\xi|y')]b_4(y'), \tag{16a}$$

$$G_4(\xi) = -4\sqrt{2\pi}\,e^{-|\xi|h}\sin(|\xi|a)[(1+|\xi|h)\cosh(|\xi|y') - |\xi|y'\sinh(|\xi|y')]b_4(y'), \tag{16b}$$

where "+" in eqn (16a) refers to $\xi > 0$ and "−" refers to $\xi < 0$.

The expressions for $F_2(\xi)$, $G_2(\xi)$, $F_4(\xi)$ and $G_4(\xi)$ were arrived at by carrying out the Fourier integration (along $-\infty < x < \infty$, $y = h$) of the Muskhelishvili (1963) complex potentials associated with the dislocations in an infinite medium. Then, real and imaginary parts of the appropriate combinations of the transformed potentials are extracted.

Substitution of the respective forms for $F(\xi)$ and $G(\xi)$ into eqns (13) leads to expressions involving single integrals along $0 < \xi < \infty$ for the stresses $\sigma_F(z)$, $\sigma_{2R}(z,x')$ and $\sigma_{4R}(z,y')$. These integrals were evaluated using a combination of Laguerre and Filon integration [see Abromowitz and Stegun (1964)]. In particular, each component of stress involves a summation of terms of the form:

$$\text{stress component} = \sum_m A_m \int_0^\infty \begin{Bmatrix}\sin(\xi_m w)\\ \cos(\xi_m w)\end{Bmatrix} e^{-w} f_m(w)\,dw.$$

For $\xi_m > 1$, the Filon formula was used (with $\theta = 0.5$), while for $\xi_m < 1$, 15-point Laguerre integration was used. The numerical integration converges rapidly because both the dislocation pair and quadruple, being akin to diples, have stresses which decay rapidly as $|x| \to \infty$. The stresses so computed form part of the integrands in eqn (4). Coupled singular

integral equations (of the Cauchy type) can then be derived for the unknown densities $b_2(x')$ and $b_4(y')$ by enforcing $\sigma_{yy} = 0$ on $-s < x < s, y = 0$, and the interface law on $x = \pm a$. In other words, just evaluating the *kernels* of these integral equations necessitates a numerical integration over $0 < \xi < \infty$. The overall procedure is similar to that used by Ballarini *et al.* (1984) in their study of a crack propagating transverse to a beam.

A relatively standard collocation procedure is used to solve the integral equations numerically. The to-be-determined dislocation densities are interpolated in a continuous, piece-wise linear fashion between discrete points; the values of the densities at the discrete points constitute the finite number of unknowns. The results to be shown are based on 15 unknowns along $-s < x < s, y = 0$, and 30 unknowns along $x = 0$, $d < y < h$, where d is the current position of the end of the debond.

Besides the extensive comparisons with the results of Method II, we also tested Method I by computing the stress intensity factor for an infinite strip which contains a pressured-open, finite crack running parallel to the strip. This involves only the use of dislocations along $-a < x < a$. We compared our computed stress intensity factors with those given in graphical form in Tada *et al.* (1973), and negligible differences were found. This comparison suggests that at least part of our method is working properly, in particular that the integrals defined in the Appendix are being evaluated accurately. Since the solution of this crack problem does not involve dislocations along $x = \pm a$, comparisons with Method II are necessary to have some indication as to whether these are being computed properly. It is also worth mentioning, however, that the results of Ballarini *et al.* (1989) further support the accuracy of this type of singular integral equation technique in solving problems involving interfacial slippage.

Method II

A multi-domain BEM program employing isoparametric quadratic elements was also developed to analyse the present problem. The standard BEM formulation for solving a linear elastic problem is applied to each of the two subdomains, the fiber and the matrix, respectively (Anderson, 1981; Brebbia *et al.*, 1984; Karami and Fenner, 1986; Achenbach and Zhu, 1989). The boundary integral equation governing the displacement at the point P on the boundary of an isotropic linearly elastic subregion $\Omega^{(k)}$ can be written as:

$$C_{ij}^{(k)}(P)u_j^{(k)}(P) + \int_{\Gamma^{(k)}} S_{ij}^{(k)}(P, Q)uj^{(k)}(Q)\,\mathrm{d}\Gamma = \int_{\Gamma^{(k)}} U_{ij}^{(k)}(P, Q)Tj^{(k)}(Q)\,\mathrm{d}\Gamma, \tag{17}$$

where $\Gamma^{(k)}$ is the boundary of the subdomain $\Omega^{(k)}$, and $S_{ij}^{(k)}$ and $U_{ij}^{(k)}$ are the fundamental traction and displacement solutions, respectively. $C_{ij}^{(k)}(P)$ is the rigid body translation solution of (17), and it depends on the geometry of the boundary at point P; in particular, $C_{ij}^{(k)}(P) = \delta_{ij}/2$ for smooth boundaries, where δ_{ij} is the Kronecker delta. The fundamental solutions $S_{ij}^{(k)}$ and $U_{ij}^{(k)}$ can be found in Brebbia *et al.* (1984). Physically, they represent the traction and displacement in the jth direction at a point Q due to a unit force acting in the ith direction at a point P.

In our formulation, the fiber and the matrix occupy separate domains so that a point P on the fiber–matrix interface is shared by both domains. These points on the interface will be denoted by P_{lf} and P_{lm} respectively; $(P_{\mathrm{lf}}, P_{\mathrm{lm}})$ are called nodal pairs when the boundary is discretized. The same quadratic shape functions are used to interpolate the geometry, displacements and tractions for the points between the nodal points on the boundary of each domain. Using these interpolation functions, (17) can be integrated element by element resulting in the following matrix equations for each subdomain:

$$[H^{(k)}]\{u^{(k)}\} = [G^{(k)}]\{T^{(k)}\}, \tag{18}$$

where $[H^{(k)}]$ and $[G^{(k)}]$ are the matrix operators corresponding to the traction and displacement kernels $S_{ij}^{(k)}$ and $U_{ij}^{(k)}$, respectively; $\{u^{(k)}\}$ and $\{T^{(k)}\}$ are the nodal displacement and nodal traction vectors, respectively.

Symmetry considerations allow us to consider only half of the specimen, i.e. $x > 0$, so that there are only two subdomains in our problem. Furthermore, we have truncated the domain so that the matrix occupies the region $a < |x| < b$. (In practice, we took $b/a = 25$.) The two sets of linear algebraic equations corresponding to each subdomain are then coupled together via the interface model and solved simultaneously. Specifically, let Ω^f denote the subregion occupied by the fiber and Ω^m denote the matrix. For subdomain Ω^f, we define the following:

u^f, T^f—nodal displacements and tractions at the boundary other than the interface,
u_I^f, T_I^f—nodal displacements and tractions at the interface.

For subdomain Ω^m we define the following:

u^m, T^m—nodal displacements and tractions at the boundary other than the interface,
u_I^m, T_I^m—nodal displacements and tractions at the interface.

From (18), for subdomain Ω^f, we have

$$[H^f \quad H_I^f]\begin{Bmatrix} u^f \\ u_I^f \end{Bmatrix} = [G^f \quad G_I^f]\begin{Bmatrix} T^f \\ T_I^f \end{Bmatrix}. \tag{19}$$

Similarly for subdomain Ω^m, we have

$$[H^m \quad H_I^m]\begin{Bmatrix} u^m \\ u_I^m \end{Bmatrix} = [G^m \quad G_I^m]\begin{Bmatrix} T^m \\ T_I^m \end{Bmatrix}. \tag{20}$$

At the interface, force equilibrium dictates that

$$T_I^f = -T_I^m = T^I. \tag{21}$$

Consistent with the interface model, the displacements will not, in general, be continuous across the interface. Combining (18)–(21), we obtain the following system of equations:

$$\begin{bmatrix} H^f & H_I^f & -G_I^f & 0 & 0 \\ 0 & 0 & G_I^m & H^m & H_I^m \end{bmatrix}\begin{Bmatrix} u^f \\ u_I^f \\ T^I \\ u^m \\ u_I^m \end{Bmatrix} = \begin{bmatrix} G^f & 0 \\ 0 & G^m \end{bmatrix}\begin{Bmatrix} T^f \\ T^m \end{Bmatrix}. \tag{22}$$

After imposing the boundary conditions on the elements other than those on the interface, we find that (22) is underdetermined, i.e. there are more unknowns that equations. This situation is remedied by using the relevant relations derived from the interface model. For instance, in the pure frictional sliding case, if there is no relative slip, then at a generic node pair (P_{If}, P_{Im}), $u_I^f(P_{If}) = u_I^m(P_{Im})$. On the other hand, $T_{xy}^I = \pm\mu|T_{xx}^I|$, if the boundary points slip with respect to each other.

Notice that although the interface behavior is nonlinear, the two subregions themselves remain elastic throughout the entire deformation process. The boundary integral equation (17) is valid if the tractions and displacements are replaced by the traction rates and displacement rates, respectively; this forms the basis of an incremental formulation (Andersson, 1981; Karami and Fenner, 1986).

Since the extent of the slip region is not known in advance, the problem has to be solved iteratively. A direct iteration method is used. For the interface described by Coulomb friction alone (no bonding), the program first computes the stress field everywhere assuming no slip on the interface, for a given applied pressure p. For any point on the interface, the program then checks whether the interfacial shear stress exceeds the shear

limit which is the product of the interfacial normal stress at the point and the friction coefficient. If the shear limit is exceeded, the shear stress at that point is set equal to the shear limit. If it is smaller than the shear limit, displacement continuity prevails. Using these contact conditions, the problem is solved again with the same load p. This process is repeated until the solution converges, i.e. there is no further change in the contact conditions.

For the combined debonding and frictional sliding case, the program performs basically the same tasks as described above. However, an additional check associated with the relative slippage δ on the fiber–matrix interface must be made. Specifically, the shear limit corresponds to the cohesive resistance τ^* if $\delta < \delta^*$, whereas it is given by the Coulomb friction law if $\delta > \delta^*$. An algorithm for handling the unloading problem (decreasing p) is given by Wang *et al.* (1991).

4. RESULTS AND COMPARISON WITH APPROXIMATE FORMULAE

The model problem considered here displays a response to the applied load which is similar to the response of the real composite specimen. Initially, the applied pressure causes purely elastic deformation of the strip. Once the cohesive shear stress τ^* is first reached, relative motion at the interface begins; the cohesive stress is first reached at the point where the interface intersects the free surface. Under increasing applied load, the relative displacement at the surface increases and the extent of the interface which has reached the cohesive stress increases. When the relative displacement at the surface exceeds δ^*, debonding is said to have initiated. The load may then drop temporarily, depending on interface parameters, but in any event the debond extends. Of interest is how the applied load varies as the debond propagates, and how this variation depends on interface parameters, including the presence or absence of bonding.

In Fig. 3 we display typical results for the purely Coulomb friction interface and for an interface characterized by debonding according to a cohesive zone law followed by Coulomb friction. The following parameters were used: $h = 25a$, $s = 4a$, $\mu = 0.1$, $\sigma_0/E = 4 \times 10^{-5}$, $\tau^*/E = 8 \times 10^{-6}$, $\delta^*/E = 2.5 \times 10^{-5}$, $\nu = 0.25$. The cohesive zone is defined at that portion of the interface where relative displacement of the interface has begun but has not reached δ^*; in the frictional slip zone, the relative displacement has exceeded δ^*. For the interface with bonding, the cohesive zone extends from $y = 13.25a$ to $y = 14.75a$, and the frictional slip zone is from $y = 14.75a$ to $y = 25a$ (the top of the specimen where

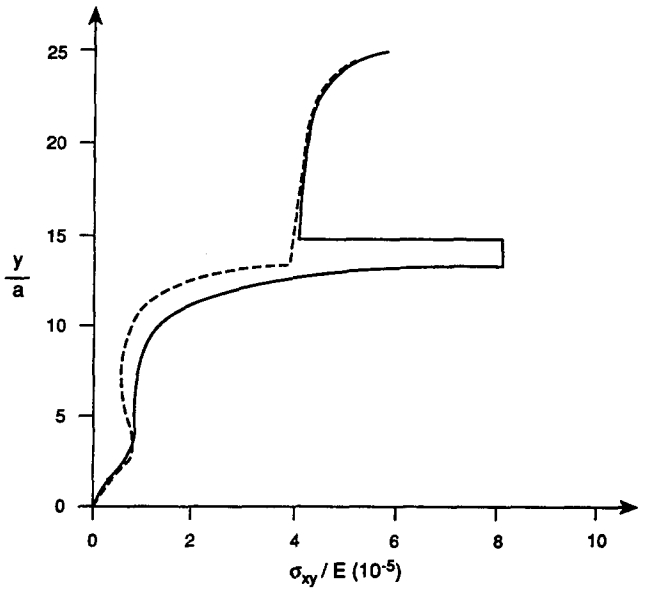

Fig. 3. Typical distribution of interfacial shear stress for bonded and purely frictional interface ($h = 25a$, $s = 4a$, $\mu = 0.1$, $\sigma_0/E = 4 \times 10^{-5}$, $\tau^*/E = 8 \times 10^{-6}$, $\delta^*/a = 2.5 \times 10^{-5}$, $\nu = 0.25$).

the load is applied). For the purely frictional interface, there is no cohesive zone, and the frictional slip zone is from $y = 13.25a$ to the top. As expected, for the interface with bonding, the shear stress is equal to $\mu|\sigma_{xx}|$ in the slip zone and τ^* in the cohesive zone; the shear stress is less than τ^* in the bonded portion ($y < 13.25a$). On the other hand, for the purely frictional interface, the shear stress is equal to $\mu|\sigma_{xx}|$ in the slip zone and less than $\mu|\sigma_{xx}|$ in the unslipped portion.

The results shown in Fig. 3 are for the case of identical elastic moduli; they were arrived at using method I, which is based on distributed dislocations. For the same set of material and loading parameters, Method II (a modified boundary integral equation method) yielded results which agreed to within 2%. Such agreement between the two methods was consistently obtained, except when the cohesive zone had nearly reached the bottom of the specimen, in which case Method I was viewed as somewhat more likely to be accurate. On the other hand, method II was necessary to assess the influence of having dissimilar constituent moduli.

The variation of the shear stress along the interface shown in Fig. 3 suggests an approximate analysis which is based on modifying the simple constant shear stress approximation (often used in the composite materials literature) to account for the cohesive zone. Let the cohesive zone occupy the region from $d < y < d+h^*$; the interfacial shear stress is equal to τ^* in this zone. Above that zone, the shear stress is equal to $\mu\sigma_0$. If, in addition, we assume that the fiber load is zero at $y = d$, then the pressure applied to the fiber by the indentor is given by

$$p = \mu\sigma_0\left(\frac{L-h^*}{a}\right)+\tau^*\frac{h^*}{a}, \tag{23}$$

where $L = h-d$ is the total extent of the interface on which there is relative displacement; it is the sum of the lengths of the frictional slip zone ($L-h^*$) and the cohesive zone (h^*).

The cohesive zone length h^* is determined by the condition that the relative displacement at the top of the cohesive zone is equal to δ^*; i.e. $\delta(d+h^*) = \delta^*$. If we neglect deformation in the matrix, and approximate the fiber strain as uniform in x for fixed y, then this leads to the following equation for h^*:

$$h^* = \sqrt{\frac{2E_f'\delta^* a}{\tau^*}}, \tag{24}$$

where $E_f' = E_f/(1-\nu_f^2)$ appears because of the plane strain condition. The indentor pressure, therefore, is given approximately by

$$p = \mu\sigma_0\left[\frac{L}{a}-\sqrt{\frac{2E_f'\delta^*}{\tau^* a}}\right]+\sqrt{\frac{2E_f'\tau^*\delta^*}{a}}. \tag{25}$$

We consider now the numerical results based on a rigorous implementation of the cohesive zone model for interfacial debonding. Insight into these results will be gained by comparing them with the results of two other analyses: that which leads to the approximate equation (25) and a rigorous implementation of debonding according to linear elastic fracture mechanics (LEFM). In LEFM, the elastic energy released by extension of the debond must be sufficient to supply the energy required to debond the interface. This is the approach suggested by Marshall and Oliver (1987) for the push-in test, who also put forth an approximate analysis of the energy balance. The LEFM approach might be more readily recognized by its accounting for the stress singularity at the tip of the debond; in the present situation, the friction along the interface behind the debond tip contributes to the magnitude of the stress singularity at the tip, as does the applied load. To connect the LEFM approach to debonding with that based on a cohesive zone model, it is important to recall the

equivalence found by Rice (1969): LEFM and a cohesive zone model give identical predictions—with the critical energy release rate G_d equal to the area under the curve of cohesive stress versus relative displacement—if the cohesive zone size is small compared with all other length scales.

In the present problem, there are three relevant length scales: the size of the cohesive zone; the fiber radius and the debond length L. This prompts the definition of the following parameter Φ:

$$\Phi = \sqrt{\frac{\delta^* E_f'}{\tau^* a}} = \sqrt{\frac{(\delta^*)^2 E_f'}{G_d a}}, \tag{26}$$

where $G_d = \tau^* \delta^*$ for our simple cohesive stress–relative displacement curve. By appealing to the approximate result (24), the parameter Φ is seen to be proportional to (h^*/a): the size of the cohesive zone relative to the fiber radius.

Consider now the variation of load with debond length as a function of τ^* and δ^* holding the product $G_d = \tau^* \delta^*$ fixed. (We continue to take the fiber and matrix moduli to be equal.) Plotted in Fig. 4 is the dimensionless pressure $p\sqrt{a}/\sqrt{\tau^* \delta^* E_f'}$ as a function of debond length for $\Phi = 23$ and $\Phi = 1.6$, and for two different specimen thicknesses. The frictional parameters are $\mu = 0.3$ and $\sigma_0\sqrt{a}/\sqrt{\tau^* \delta^* E_f'} = 0.054$. The solid curves represent the numerical results, and the approximation (25) is represented by the dashed curves. (For the case of $\Phi = 23$, the solid curves for the two specimen thicknesses are indistinguishable.) As indicated above, calculations were also carried out with debonding modeled, not by a cohesive zone law, but by LEFM. Debonding in this case is described simply by the mode II critical energy release rate G_d; sliding after debonding is still modeled by Coulomb friction. These LEFM-based calculations, represented in Fig. 4 by the single dotted curve, were for a specimen of infinite thickness ($h \to \infty$).

The conclusions to be drawn from Fig. 4 are not unexpected: If Φ is much greater than 1, the cohesive zone model and LEFM lead to significantly different results regardless of the length of the debond. Their respective results appear to approach each other, however, as Φ decreases; even Φ near one produces reasonable agreement between the models, provided the debond length L is sufficiently long (at least several fiber radii). By contrast, for relatively large Φ, the approximate analysis which leads to (25) agrees rather well with the more detailed analysis, though, as discussed further below, the frictional contribution is likely to require modification.

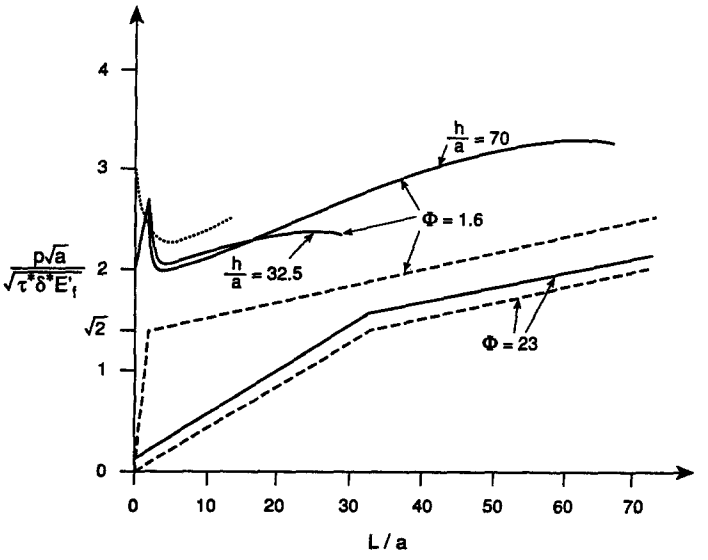

Fig. 4. Predicted pressure versus debond length (——— ~ detailed numerical analysis; ---- ~ approximate analysis; ··· ~ LEFM).

Consider the approximation (25) in the limit of $\Phi \to 0$:

$$p = \mu\sigma_0 \frac{L}{a} + \sqrt{\frac{2E_f'G_d}{a}}. \tag{27}$$

This result, were it accurate, could be quite useful in interpreting experimental data. It states that the *change* in the load with debond propagation depends only on the friction, while the load obtained by extrapolating back to zero debond length depends only on the bonding. It must be pointed out that this result is precisely the two-dimensional analog of that given by Marshall and Oliver (1987), who used an approximate energy balance to analyse the fiber push-in problem. In terms of our variables, their analysis assumed that the load must overcome an interfacial debonding energy G_d, as well as *constant* frictional resistance $\mu\sigma_0$. Unfortunately, as indicated by the curves corresponding to $\Phi = 1.6$ in Fig. 4, the approximation (27), which is represented by the dashed curve (displaced slightly upwards so that the intercept on the vertical axis is $\sqrt{2}$), is not very accurate for the set of parameters considered here.

It is worth commenting further on the accuracy of the Marshall and Oliver approximation—for our present purposes, eqn (27)—in the limit of small Φ, particularly since such an approach continues to be championed as accurate for long debond lengths (Evans and Marshall, 1989). In fact, much insight can be gained from continuing to consider the idealized problem of a planar geometry, now simply a uniformly pressured fiber in an infinite half-plane ($h \to \infty$), with equal fiber and matrix moduli. Afterwards, we will comment on the likely influence of three-dimensionality and dissimilar constituent moduli. In Fig. 5 we plot the dimensionless fiber pressure $p\sqrt{a}/\sqrt{G_d E_f'}$ as a function of the debond length; debonding at the interface is modeled with a critical energy release rate (LEFM), and subsequent sliding is governed by Coulomb friction. Note that the curves correspond to several different values of the dimensionless parameter $\sigma_0\sqrt{a}/\sqrt{G_d E_f'}$, which captures the relative magnitudes of frictional and debonding resistance: for small values of this parameter, the frictional resistance is low in comparison with the debonding resistance. All curves are for $\mu = 0.3$, except for the single curve labelled $\mu = 0$.

Several features of Fig. 5 deserve attention. First, for relatively long debonds, the load versus debond length is asymptotic to a linear function for long debonds. To aid in the discussion, we imagine the linear portions of each curve extrapolated back to $L/a = 0$. Thus, if we are concerned only with long debonds, it is sufficient to describe the function

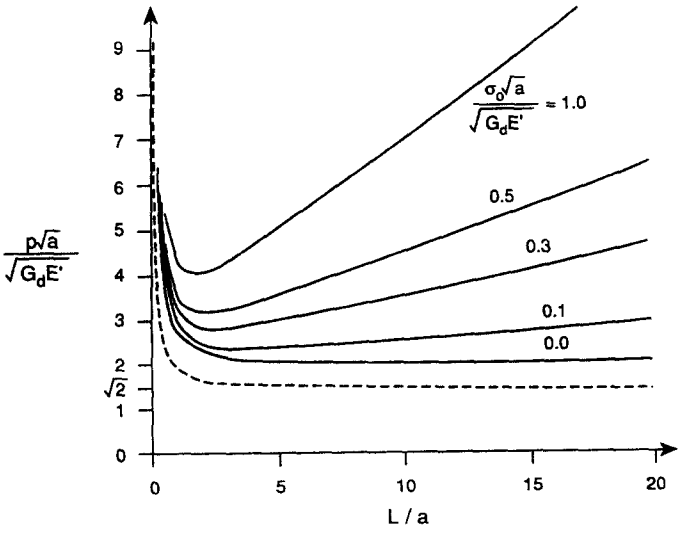

Fig. 5. Pressure versus debond length using LEFM, indicating effect of Coulomb friction (——— ~ $\mu = 0.3$; ----- ~ $\mu = 0.0$).

of load versus debond length by a slope and an intercept (at $L/a = 0$). Consider first the curves for which $\sigma_0\sqrt{a}/\sqrt{G_d E_f'} > 0$. It is quite clear that the back-extrapolated intercept depends on the parameter $\sigma_0\sqrt{a}/\sqrt{G_d E_f'}$; if eqn (27) were accurate, then all curves would extrapolate back to $p\sqrt{a}/\sqrt{G_d E_f'} = \sqrt{2}$.

The origin of the discrepancy can be seen by considering the remaining curves: $\mu = 0$, and $\sigma_0\sqrt{a}/\sqrt{G_d E_f'} = 0$ with $\mu = 0.3$. For $\mu = 0$, the numerical results for long debonds agree with eqn (27). This result could be arrived at by an even simpler argument: the energy released when the two crack tips extend a unit distance is precisely equal to the strain energy of a block of width $2a$ and unit length, which is subjected to uniaxial plane strain compression p. On the other hand, when $\mu = 0.3$ and $\sigma_0\sqrt{a}/\sqrt{G_d E_f'} = 0$, the back-extrapolated load is greater than $\sqrt{2}$. Even though the nominal friction stress $\mu\sigma_0$ is zero, the Poisson expansion of the fiber leads to interfacial compression just behind the debond tip; since the friction coefficient is nonzero, the load necessary to produce an adequate energy release rate is higher than if μ were equal to 0. In particular, one expects the back-extrapolated load for $\sigma_0\sqrt{a}/\sqrt{G_d E_f'} = 0$ to increase monotonically with μ. Note, however, that the back-extrapolated load differs from $\sqrt{2}$ by roughly 50% even for the not unreasonable value $\mu = 0.3$.

These findings serve to emphasize the point made by Dollar and Steif (1988) based on their two-dimensional analysis of the push-in test: If the interface is characterized by Coulomb friction, then the response depends not only on the product $\mu\sigma_0$, but also on the individual parameters. Furthermore, in the limit of very small μ, but $\mu\sigma_0$ still on the order of p, the results of the constant shear stress approximation, which ignore Poisson expansion of the fiber, are reasonably accurate. Hence, we can say that the Marshall and Oliver approximation—or our eqn (27)—is accurate if the friction coefficient is very small and, as they point out, if the debond is long. A recent study of the push-out test by Liang and Hutchinson (1992) also has the debonding contribution essentially decoupled from the frictional contribution, largely because a detailed analysis combining Coulomb friction and the fracture problem was not carried out.

Continuing to focus on the limit of $\Phi \to 0$, in which the fracture mechanics approach to debonding becomes equivalent to the cohesive zone approach, we offer some remarks as to the likely influence of three-dimensionality and dissimilar fiber and matrix moduli. Considering first the limit of very small friction coefficients, we propose that the separation of debonding and frictional contributions to the load will continue to hold for long debonds. The debonding contribution—related to the back-extrapolated initial load—can be computed via an energetic argument identical to the one given above: the energy released is the difference between the energy in the fiber far ahead of the debond (namely, zero) and the energy in the fiber far behind. A calculation of this type has been done by Hutchinson and Jensen (1990) for the pull-out problem. The frictional contribution will be linear just as in Marshall and Oliver's calculation, with no dependence on the elastic moduli.

For nonvanishing friction coefficients, we would claim that the Marshall and Oliver result—or the three-dimensional version of our eqn (27)—will be incorrect for two reasons. First, as illustrated in Fig. 5, the back-extrapolated load will not be given by the energy release calculation because of the load-induced normal pressure at the interface just behind the debond. Secondly, the variation of load with debond length will not be linear if the interface is characterized by Coulomb friction with a nonvanishing friction coefficient. This is implicit in the work of Shetty (1988), who adapted the shear-lag analysis of Takaku and Arridge (1973) to the push-out test; Shetty's analysis leads one to conclude that the load increases *exponentially* with the slip length (and with the friction coefficient and a parameter containing the elastic moduli). By carrying out detailed calculations with an integral equation method and a finite element method, Meda *et al.* (1991) found that this exponential variation of load with slip length was quite accurate.

To expand on some of the above points, we present in Fig. 6 specific results for dissimilar fiber and matrix moduli. These results are for the two-dimensional push-out test ($h/a = 25$) and were arrived at using Method II. (The jaggedness of the curves is associated with the coarseness of the mesh and the finite size of the load step.) While the modulus

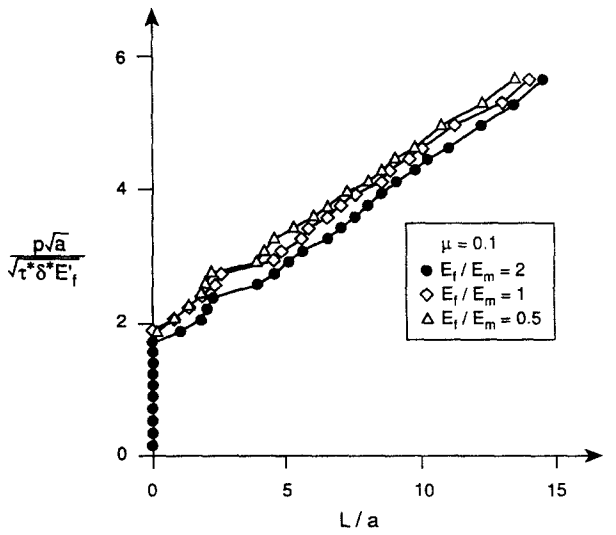

Fig. 6. Pressure versus debond length for various relative moduli E_f/E_m.

ratio E_f/E_m has been varied, the Poisson ratios ν_f and ν_m have been fixed at 0.25, and the other parameters are: $\mu = 0.1$, $\sigma_0/E_f = 4 \times 10^{-5}$, $\tau^*/E_f = 8 \times 10^{-6}$, $\delta^*/a = 2.5 \times 10^{-5}$; therefore, the parameter $\sigma_0\sqrt{a}/\sqrt{\tau^*\delta^*E_f'}$ has the value 2.74. The cohesive zone parameters correspond to a relatively small value of Φ ($\Phi \approx 1.7$), so the results are relevant to the situation in which debonding is captured with fair accuracy by LEFM. The first point to be made is that the back-extrapolated load is greater than $\sqrt{2}$. It is less, however, than the values typical of Fig. 5, probably because of the lower friction coefficient.

It can also be seen that the variation of the load with E_f/E_m for fixed L/a is relatively modest. This had to be expected in this problem involving a *planar strip*. The Poisson effect—namely the normal stress induced at the interface due to the fiber Poisson expansion—will be relatively small because the net axial force in the x-direction across the whole strip cannot be altered by the load applied to the fiber; that is,

$$\frac{1}{h}\int_0^h \sigma_{xx}\,dy = -\sigma_0.$$

Since the induced normal stress is compressive in the upper portion of the strip and tensile in the lower portion, there will be some Poisson effect when the slip zone extends only over a portion of the interface. Once the entire interface is slipping, however, the average friction stress along the interface will be $\mu\sigma_0$. Note that this constraint on the induced normal force is not present in the half-plane problem, nor in the three-dimensional problem, irrespective of whether the domain is of finite or infinite thickness.

We now consider relatively large values of the parameter Φ and, in particular, its effect on the sensitivity to the fiber–matrix modulus ratio. It should be apparent that the change in the load as the debond propagates is tied to the friction; furthermore, as just explained, two-dimensional calculations on a sample of finite thickness predict little if any alteration in the friction stress with modulus ratio. Therefore, we focus on the degree to which initial debonding depends on the modulus ratio. We are not referring here to a pressure intercept obtained by back-extrapolation based on the linear asymptotic behavior for long debonds. We are referring to the actual initiation of debonding, for example, the local pressure peaks that appear towards the left end of Fig. 4 ($\Phi = 1.6$). Initiation is predicted to occur at a definite pressure when using the cohesive zone model, while a finite initiation pressure is obtained in LEFM only if some initial debond length is assumed. The initial debond pressure is that required to first achieve a relative displacement δ^* on the surface.

Table 1. Dimensionless debond pressure $p_{\text{init}}\sqrt{a}/\sqrt{\tau^*\delta^* E_f'}$ for several values of Φ and E_f/E_m

Φ	$E_f/E_m = 0.5$	$E_f/E_m = 1.0$	$E_f/E_m = 3.54$
5.80	1.97	2.19	2.83
36.3	1.59	1.66	1.95
145.1	1.49	1.52	1.65

Results for the dimensionless initial debond pressure $p_{\text{init}}\sqrt{a}/\sqrt{\tau^*\delta^* E_f'}$ are displayed in Table 1 for several values of Φ and modulus ratio E_f/E_m; these are based on fixing the parameter $\tau^*\delta^*/aE_f'$ (a dimensionless debond energy) at the value 8.04×10^{-8}. According to the approximate solution (25), the dimensionless initiation pressure is equal to $\sqrt{2} \approx 1.41$, irrespective of Φ and E_f/E_m. One can see that this approximate result is approached as Φ increases, and also that the variations associated with different values of E_f/E_m decrease as Φ increases. Thus, if large values of Φ are appropriate, the shear-lag approximation will probably be reasonable, at least as far as initiation is concerned.

5. CONCLUSIONS

A detailed stress analysis of a two-dimensional analog to the fiber push-out problem has been carried out. Two distinct methods of analysis were employed; the similarity in the results suggests that the results are rather accurate. The analyses have been carried out under the assumption that the interface can be characterized by a Barenblatt-type cohesive zone model to capture initial debonding. Frictional sliding subsequent to debonding is modeled with a Coulomb friction interface law.

We have found two distinct regimes of response: one in which the cohesive zone size is of the order of, or small compared with, the fiber diameter and one in which the cohesive zone size is large compared with the fiber diameter. For relatively small cohesive zones, the results of our analyses are essentially equivalent to those arrived at using linear elastic fracture mechanics to model interfacial debonding. In this limit, approximate, shear-lag style analyses may capture the change in indentor load with debond extension, this change being associated with the frictional resistance. However, they are unlikely to offer an accurate estimate of the absolute level of the indentor load, at least when there is a non-negligible friction coefficient. By contrast, when the cohesive zone is relatively large and linear elastic fracture mechanics is inappropriate, a shear-lag style analysis—possibly altered in the spirit of the Shetty (1988) analysis to include the effects of Coulomb friction—can capture the variation in the indentor load with satisfactory accuracy. The results of an effort to interpret the push-out data by Eldridge *et al.* (1991) using a cohesive zone model for debonding are being simultaneously reported (Dollar and Steif, 1992).

Acknowledgements—A.D. and P.S.S. were supported by the Department of Energy under grant DE-FG02-89ER45404, by General Electric Aircraft Engines, and by the Department of Mechanical Engineering, Carnegie Mellon University. Y.C.W. and C.Y.H. were supported by the Cornell Materials Science Center which is funded by the NSF/DMR/MRL program.

REFERENCES

Abromowitz, M. and Stegun, I. A. (1964). *Handbook of Mathematical Functions*. National Bureau of Standards, Washington, DC.

Achenbach, J. D. and Zhu, H. (1989). Effect of interfacial zone on mechanical behavior and failure of fiber reinforced composites. *J. Mech. Phys. Solids* **37**, 381–394.

Andersson, T. (1981). Boundary element methods. In *Proc. 3rd Int. Seminar*, Irvine, CA (Edited by C. A. Brebbia), pp. 239–258. Springer, Berlin.

Ballarini, R., Ahmed, S. and Mullen, R. L. (1989). Finite element modeling of frictionally restrained composite interfaces. In *Interfaces in Metal-Ceramic Composites* (Edited by R. Y. Lin, R. J. Arsenault, G. P. Martins and S. G. Fishman), pp. 349–389. The Minerals, Metals and Materials Society.

Ballarini, R., Shah, S. P. and Keer, L. M. (1984). Crack growth in cement-based composites. *Engng Fract. Mech.* **20**, 433–441.

Barenblatt, G. I. (1962). The mathematical theory of equilibrium of cracks in brittle fracture. *Adv. Appl. Mech.* **7**, 55–129.
Brebbia, C. A., Telles, J. C. F. and Wrobel, L. C. (1984). *Boundary Element Techniques*. Springer, Berlin.
Bright, J. D., Shetty, D. K., Griffin, C. W. and Limaye, S. Y. (1989). Interfacial bonding and friction in silicon carbide (filament)-reinforced ceramic- and glass–matrix composites. *J. Am. Ceram. Soc.* **72**, 1891–1898.
Brun, M. K. and Singh, R. N. (1988). Effect of thermal expansion mismatch and fiber coating on the fiber/matrix interfacial shear stress in ceramic matrix composites. *Adv. Ceram. Mater.* **3**, 506–509.
Deshmukh, R. V. and Coyle, T. W. (1988). Determination of the interface strength in glass–SiC composites via single fiber tensile testing. *Ceram. Engng Sci. Proc.* **9**, 627–634.
Dollar, A. and Steif, P. S. (1988). Load transfer in composites with a Coulomb friction interface. *Int. J. Solids Structures* **24**, 789–803.
Dollar, A. and Steif, P. S. (1989). A tension crack impinging upon frictional interfaces. *J. Appl. Mech.* **56**, 291–298.
Dollar, A. and Steif, P. S. (1992). A cohesive zone approach to interpreting the fiber push-out test. *J. Am. Ceram. Soc.* (to appear).
Eldridge, J. I., Bhatt, R. T. and Kiser, J. D. (1991). Investigation of interfacial shear stength in SiC/Si_3N_4 composites. *Ceram. Engng Sci. Proc.* **12**, 1152–1171.
Evans, A. G. and Marshall, D. B. (1989). The mechanical behavior of ceramic matrix composites. *Acta Metall.* **37**, 2567–2583.
Grande, D. H., Mandell, J. F. and Hong, K. C. C. (1988). Fiber-matrix bond strength studies of glass, ceramic and metal matrix composites. *J. Mater. Sci.* **23**, 311–328.
Griffin, C. W., Shetty, D. K., Limaye, S. Y. and Richerson, D. W. (1988). Evaluation of interfacial properties in borosilicate-SiC composites using pullout test. *Ceram. Engng Sci. Proc.* **9**, 671–687.
Hutchinson, J. W. and Jensen, H. M. (1990). Models of fiber debonding and pullout in brittle composites with friction. *Mech. Mater.* **9**, 139–163.
Laughner, J. W., Shaw, N. J., Bhatt, R. T. and DiCarlo, J. A. (1986). Simple indentation method for measurement of interfacial shear strength in SiC/Si_3N_4 composites. *10th Annual Conference on Composites and Advanced Ceramic Materials*, American Ceramic Society, Coco Beach, FL.
Liang, C. and Hutchinson, J. W. (1992). Mechanics of the fiber pushout test. Technical Report MECH-189, Harvard University.
Marshall, D. B. (1984). An indentation method for measuring matrix–fiber frictional stresses in ceramic composites. *J. Am. Ceram. Soc.* **67**, C-259–260.
Marshall, D. B. and Oliver, W. C. (1987). Measurement of interfacial mechanical properties in fiber-reinforced ceramic composites. *J. Am. Ceram. Soc.* **70**, 542–548.
Meda, G., Hoysan, S. F. and Steif, P. S. (1991). The effect of fiber Poisson expansion in micro-indentation tests. *J. Appl. Mech.* (to appear).
Muskhelishvili, N. I. (1963). *Some Basic Problems of the Mathematical Theory of Elasticity*. Noordhoff, The Netherlands.
Rice, J. R. (1969). Mathematical analysis in mechanics of fracture. In *Fracture II* (Edited by H. Z. Liebowitz), pp. 192–308. Academic Press, New York.
Shetty, D. K. (1988). Shear-lag analysis of fiber pushout (indentation) test for estimating interfacial friction stress in ceramic–matrix composites. *J. Am. Ceram. Soc.* **71**, C-107.
Sneddon, I. N. (1951). *Fourier Transforms*. McGraw-Hill, New York.
Seif, P. S. and Dollar, A. (1992). A note on models of fiber–matrix interfacial debonding. *J. Am. Ceram. Soc.* **75**, 1694–1696.
Tada, H. Paris, P. C. and Irwin, G. R. (1973). *The Stress Analysis of Cracks Handbook*. Del Research Corp., Hellertown, PA.
Takaku, A. and Arridge, R. G. C. (1973). The effect of interfacial radial and shear stresses on fibre pull-out in composite materials. *J. Phys. D: Appl. Phys.* **6**, 2038–2047.
Timoshenko, S. P. and Goodier, J. N. (1970). *Theory of Elasticity*. McGraw-Hill, New York.
Wang, Y. C. Hui, C. Y., Lagoudas, D. and Papadopoulos, J. (1991). Small-scale crack blunting at a bimaterial interface with Coulomb friction. *Int. J. Fract.* **52**, 293–306.

APPENDIX

In this Appendix, the integrals introduced in eqns (13) are defined:

$$I_1(x) = \int_0^\infty G(\eta)\frac{\eta}{2\eta+\sinh 2\eta}\cosh(x\eta)\cos\left(\frac{x}{h}\eta\right)d\eta,$$

$$I_2(x) = \int_0^\infty G(\eta)\frac{1}{2\eta+\sinh 2\eta}\sinh(x\eta)\cos\left(\frac{x}{h}\eta\right)d\eta,$$

$$I_3(x) = \int_0^\infty G(\eta)\frac{\eta}{2\eta+\sinh 2\eta}\sinh(x\eta)\sin\left(\frac{x}{h}\eta\right)d\eta,$$

$$H_1(x) = \int_0^\infty \frac{F(\eta)}{i}\frac{1}{2\eta+\sinh 2\eta}\cosh(x\eta)\cos\left(\frac{x}{h}\eta\right)d\eta,$$

$$H_2(x) = \int_0^\infty \frac{F(\eta)}{i} \frac{\eta}{2\eta + \sinh 2\eta} \sinh(x\eta) \cos\left(\frac{x}{h}\eta\right) d\eta,$$

$$H_3(x) = \int_0^\infty \frac{F(\eta)}{i} \frac{1}{2\eta + \sinh 2\eta} \sinh(x\eta) \sin\left(\frac{x}{h}\eta\right) d\eta,$$

$$H_4(x) = \int_0^\infty \frac{F(\eta)}{i} \frac{\eta}{2\eta + \sinh 2\eta} \cosh(x\eta) \sin\left(\frac{x}{h}\eta\right) d\eta.$$